Inclusive Positive-Pion Production in Antiproton-Neutron Interactions at 3.5 GeV/c *

E. J. B. Terreault,† D. O. Huwe, J. M. Bishop,‡ J. A. Malko,§ B. A. Munir, B. G. Reynolds,‖ F. L. Schneider, and L. J. Simonangeli
Physics Department, Ohio University, Athens, Ohio 45701
(Received 21 February 1973)

The inclusive reactions $\bar{p}n \to \pi^+X$, $2\pi^+X$ have been studied at 3.5 GeV/c in a bubble-chamber experiment. In the absence of high-energy data, no test of scaling was performed; however, the longitudinal- and transverse-momentum distributions are qualitatively similar to other "exotic" reactions at medium-high energies (12–24 GeV). To facilitate compilations the data have been parametrized empirically in terms of x and p_T. The two-particle longitudinal-momentum distributions also show familiar behavior, and a strong positive correlation appears at $x_c \simeq x_d \simeq 0$. The π^+ energy distribution agrees remarkably well with simple thermodynamic functions, but our statistics do not allow us to distinguish between Boltzmann and Bose-Einstein forms.

I. INTRODUCTION

Despite the abundance of work in recent years on inclusive reactions,[1] many questions remain unsettled, and, from the experimental point of view, many reactions unexplored yet. One such reaction is

$$\bar{p}n \to \pi^+X. \tag{1}$$

This process could, *a priori*, show special effects due to the little understood dynamics, and peculiar kinematics, of annihilations. Indeed we find that, at 3.5 GeV/c, only 7.5% of positive pions come from nonannihilation channels, essentially $\bar{p}n \to \bar{p}n\pi^+\pi^-$. Because of the large multiplicities involved in annihilation, or annihilation-dominated processes, the first logical step in the analysis of the data is the study of inclusive distributions. In fact, even in fairly low-multiplicity annihilations, it has proved exceedingly difficult, because of the kinematical overlap of numerous channels, to isolate quasi-two-body processes and analyze them in terms of exchange mechanisms.

We would also like to point out that reaction (1) satisfies the "exoticity" criterion of Chan, Hsue, Quigg, and Wang[2] for precocious scaling. This fact constitutes a motivation for presenting our data in terms of the scaling variable x[1] to facilitate comparison with future high-energy data.[3]

Finally, the consideration of the thermodynamic aspects of hadronic interactions has long been advocated by Hagedorn.[4] His model is a *high-energy* model, high energies being those where one can neglect the limitations on particle creation due to energy and momentum conservation. At 3.5 GeV/c, nucleon-antinucleon annihilation makes 2.92 GeV available in the center-of-mass system for pion creation, and it is conceivable that the pion-energy distribution could be given simply by the Bose-Einstein formula, perhaps modified to take into account the tendency of particles to carry some of the momentum of the beam and target.

II. SELECTION PROCEDURE

Our study of reaction (1) is based on a 90 000-picture antiproton exposure at 3.5 GeV/c in the Argonne National Laboratory 30-in. deuterium-filled bubble chamber. Elastic scattering results[5] and $\pi^\pm$ momentum distributions in some *exclusive* final states[6] have already been presented. The topologies of interest for our study were three and more prongs with a "spectator" proton, either unseen or with a projected length shorter than 8 cm, corresponding to a projected momentum cutoff at 250 MeV/c. Unseen spectators were treated as zero-momentum protons with errors $|\delta p_x| = |\delta p_y| = 30$ MeV/c, $|\delta p_z| = 40$ MeV/c. We have checked that the *fitted* momentum of *unseen* spectators for four-constraint fits, and the *measured* momentum of all *visible* spectators, agree with the Hulthén wave function and are isotropic. Events with nine or more prongs contribute somewhat less than 1% of the positive tracks and were not measured.

The identification of the mass of all positive particles is generally not possible in a bubble-chamber experiment. However, we were able to study our reaction, we believe without strong bias, thanks to two facts. Firstly, with increasing multiplicity, proton production becomes improbable due to the limited phase space. For 5, 6, 7, 8 prongs it was easy to eliminate proton production (2%) by kinematics and ionization. The only significant contamination is then from 3, 4 prongs. Secondly by a charge conjugation, an isospin rotation, and a space reflection (GP conservation) it is easily seen that the *inclusive* π^+ momentum spectrum from $\bar{p}n$ interactions must be forward-backward symmetric in the center-of-mass system. Of

course, in deuterium, rescattering off the "spectator," especially on the part of slow pions, can break this symmetry. We have tried to detect such an effect in Figs. 1 and 2. Figure 1 compares forward and backward π^+'s for different topologies. Some 7000 tracks fitting a proton hypothesis by kinematics and ionization have been eliminated. For five- and six-prong events there is a slight (2 s.t.d.) depletion in the backward hemisphere, but a rescattering off the "spectator" would give a maximum difference at $\cos\theta = \pm 1$, and no difference at $\cos\theta = 0$, and this is clearly not the case. The same argument for forward-backward symmetry can be made for annihilation of $\bar{p}n$ into any number of pions. In Fig. 2, we show the corresponding angular distributions from the four-constraint fits to three-pion and five-pion final states. The former are too few in number for statistical accuracy, but there is no sign of asymmetry. In the five-pion events, there could be thirteen excess events in the extreme backward direction, 1.2% of the sample. The one-constraint fits to four and six pions (not shown), though less reliable, support symmetry to this level. Constrained fits to seven- and eight-pion states have not been thoroughly studied. Therefore we fail to see a significant violation of *GP* conservation which could be due to rescattering off the "spectator."

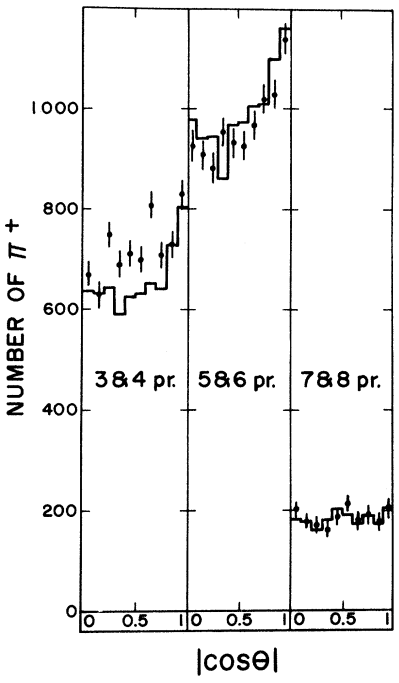

FIG. 1. The c.m. angular distributions of positive pions from different topologies. Good proton candidates have been eliminated. Histogram: forward π^+; points with error bars: backward π^+.

Returning to Fig. 1 there is a clear excess (~650 tracks) for 3,4 prongs in the backward hemisphere, which we attribute to protons. Indeed, looking at Fig. 3(a), the missing-mass plot for the hypothesis $\bar{p}\pi^- p$ MM, after subtraction of good proton fits, the peak near $MM^2 = 0$ indicates that we have let a number of protons creep in; and we have not been able to get rid of this peak by changing our acceptance criteria for a "fit." The number in the peak (~600) corresponds roughly to the backward excess in Fig. 1. However, if we select, as in the shaded histogram, Fig. 3(a), only forward particles in the c.m. system (forward when interpreted as π's), there is no obvious sign for contamination by protons. Of course, all entries with $MM^2 \gtrsim 0$ are *a priori* suspect, and, although we have included these tracks in the analysis, we have allowed for their suspicious nature in the estimation of the uncertainty on the cross section. Finally Fig. 3(b) suggests that there is little proton contamination from the final states $\pi^-\pi^-p\bar{n}$ (π^0's).

In view of these findings, we conclude with reasonable certainty that after kinematics and ionization, and, for 3, 4 prongs, after selecting forward tracks in the c.m., we have essentially all the π^+'s, and only the π^+'s; assuming *GP* conservation, the backward π^+'s which have been dropped are obtained by symmetry.

III. CROSS SECTION

The cross section was determined by computing the total track length, taking into account beam contamination. As a check, a few rolls were scanned for all interactions and gave results in agreement with the total cross section measured with counters.[7] To obtain the cross section on

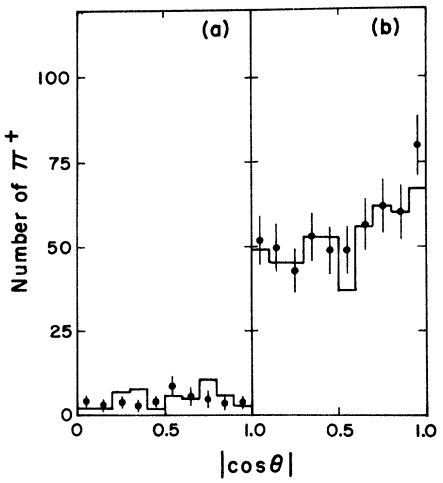

FIG. 2. The c.m. angular distributions from the events fitting (a) $\bar{p}n \to \pi^-\pi^-\pi^+$ and (b) $\bar{p}n \to \pi^-\pi^-\pi^-\pi^+\pi^+$. Histogram: forward π^+; points with error bars: backward π^+.

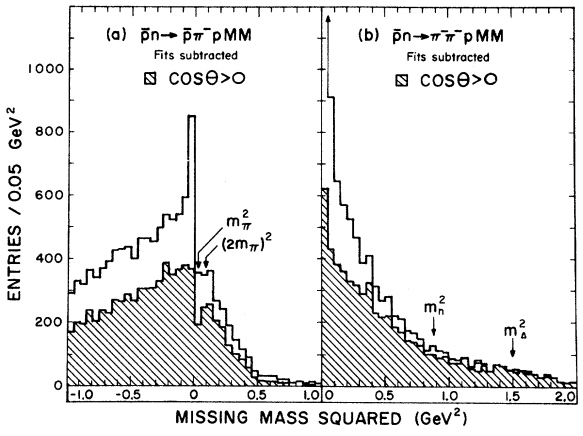

FIG. 3. Missing-mass plots for 3,4 prongs. (a) With the three outgoing tracks interpreted as $\bar{p}\pi^-p$; (b) with the three outgoing tracks interpreted as $\pi^-\pi^-p$. In both (a) and (b) events with a good fit (kinematics and ionization) to a hypothesis with a proton have been subtracted. Shaded: entries where the positive particles, interpreted as π, are forward in the c.m. system.

free-neutron targets we corrected in a conventional way[8] for screening and for high-momentum spectators, assuming a Hulthén wave function. We then get 0.77 ± 0.04 μb/event. The number of π^+ tracks used in the analysis, the number of π^+ corrected for scanning inefficiencies (~2%), measuring failures (~10%), and estimated K^+ contamination (~2%), and the corresponding π^+ production cross sections are listed by topology in Table I. Since $\sigma_{tot} = 67.8 \pm 2.7$ mb and $\sigma_{inel} = 47.1 \pm 3.6$ mb,[5] the average π^+ multiplicity is $\langle n(\pi^+)\rangle = 0.48 \pm 0.04$, and the average multiplicity per inelastic collision is $\langle n(\pi^+)\rangle_{inel} = 0.68 \pm 0.07$.

IV. SINGLE-PARTICLE MOMENTUM DISTRIBUTIONS

The single-particle invariant inclusive cross section is defined by[1]

$$f(x, p_T) = E\frac{d^3\sigma}{dp^3},$$

and after integration over the trivial azimuthal angle

TABLE I. Positive-pion production cross sections.

Topology	Number of π^+'s Used in analysis	Number of π^+'s Corrected	Cross section (mb)
3, 4 prong	6500 [a]	$14\,500^{+180}_{-1400}$ [b]	$11.2^{+0.6}_{-1.2}$ [b]
5, 6 prong	20 080	$22\,120 \pm 200$	17.0 ± 0.8
7, 8 prong	4860	5025 ± 120	3.85 ± 0.2
Total	31 440	$41\,645^{+300}_{-1400}$ [c]	$32.4^{+1.6}_{-2.2}$ [c]

[a] Forward π^+'s in the c.m. system only.
[b] Error takes into account uncertainties in eliminating protons.
[c] Including 1% for 9 and more prongs.

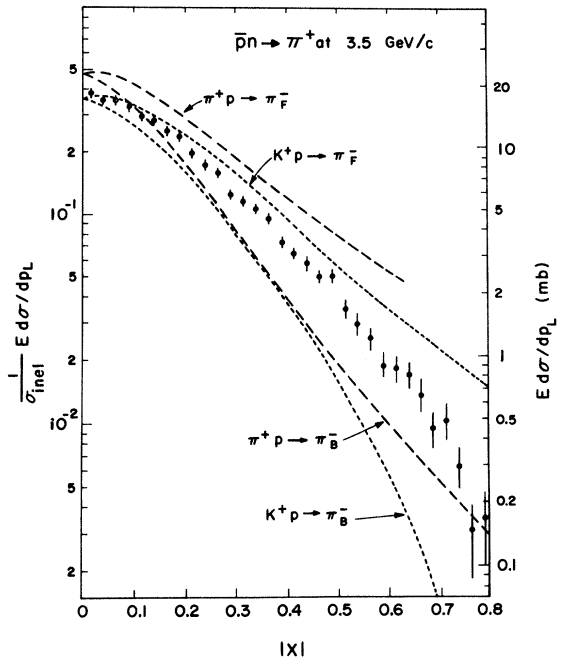

FIG. 4. The invariant distributions f (right ordinate) and f_N (left ordinate) defined in the text, as a function of $|x|$ and integrated over p_T, for our data (points) and for exotic reactions (curves, f_N only). The π^+p and K^+p data from Refs. 10, 11 have been normalized using $\sigma_{inel}(\pi^+p) = 19$ mb and $\sigma_{inel}(K^+p) = 14$ mb from Ref. 14. Subscripts F and B refer to forward and backward moving pions in the c.m. system.

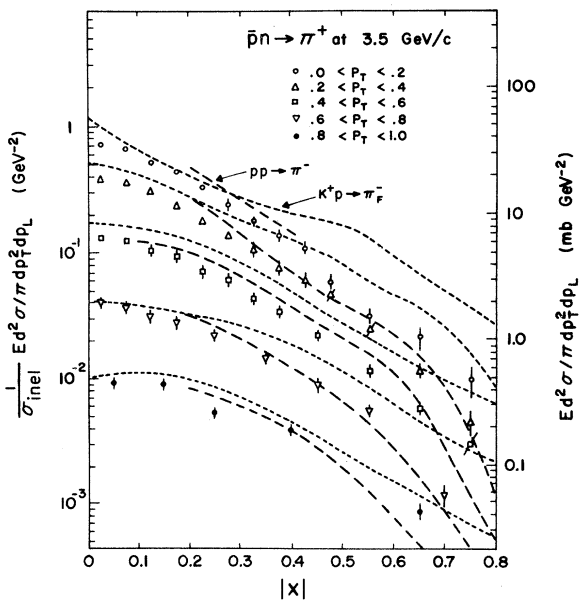

FIG. 5. The invariant distributions f (right ordinate) and f_N (left ordinate) vs $|x|$ for selected intervals of p_T, for our data (points of various shapes) and for exotic reactions (curves, f_N only). The K^+p and pp data of Refs. 12, 13 have been normalized using $\sigma_{inel}(K^+p) = 14$ mb and $\sigma_{inel}(pp) = 30$ mb from Ref. 14. The subscript F refers to forward pions in the c.m. system.

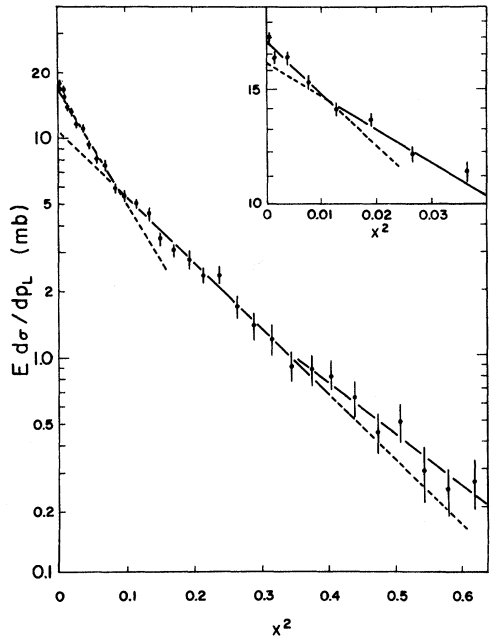

FIG. 6. The invariant distribution f vs x^2. The nearly solid lines are the results of fits to the data in certain intervals of x^2, the dashed lines extrapolations of these fits.

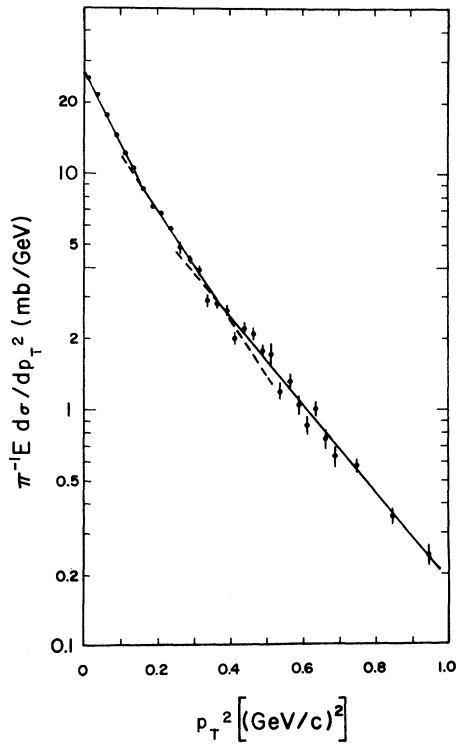

FIG. 7. The invariant distribution f vs p_T^2. The solid lines are the results of fits to the data in certain intervals of p_T^2, the dashed lines extrapolations of these fits.

$$f(x, p_T) = \pi^{-1} E \frac{d^2\sigma}{dp_T^2 dp_L}$$

$$= 2\pi^{-1} s^{-1/2} E \frac{d^2\sigma}{dp_T^2 dx},$$

where E, p_T, p_L are respectively the energy, transverse momentum, and longitudinal momentum of the particle in the c.m. system, $s^{1/2}$ the total energy in the c.m. system, and $x = 2p_L/s^{1/2}$. To compare different reactions one divides $f(x, p_T)$ by the total, or the inelastic, cross section.[1,9] Quite arbitrarily we choose the latter normalization:

$$f_N(x, p_T) = f(x, p_T)/\sigma_{\text{inel}}.$$

In Figs. 4 and 5 we display the distributions f and f_N as a function of $|x|$, in Fig. 4 integrated over p_T, and in Fig. 5 for different p_T intervals. It was immediately apparent that the shape of the distributions was qualitatively similar to those generally found in other exotic[2] reactions at higher energy. Therefore we have also shown in these figures the available data on pion production in the reactions $\pi^+ p \to \pi^-$ at 18.5 GeV/c,[10] $K^+ p \to \pi^-$ at 11.8 and 12.7 GeV/c,[11,12] and $pp \to \pi^-$ at 19.2 and 24 GeV/c.[13] As noted earlier our distributions are forward-backward symmetric by GP conservation, while the meson-induced reactions show considerable asymmetry. There is good agreement with $pp \to \pi^-$ and, interestingly with *forward* pion production in $\pi^+ p \to \pi^-$ and $K^+ p \to \pi^-$, especially at small $|x|$; however $\pi^+ p$, $K^+ p \to$ backward π^- drop

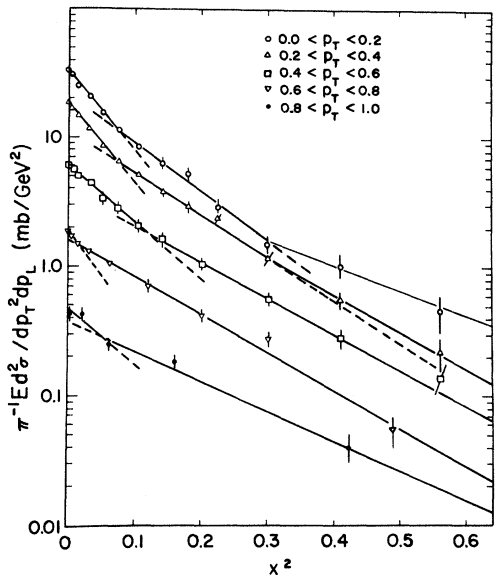

FIG. 8. The double-differential invariant distribution f vs x^2, for selected intervals of p_T. The solid lines are the results of fits to the data in certain intervals of x^2, the dashed lines extrapolations of these fits.

TABLE II. Parameters of fits to momentum distributions.

1. Fits to the longitudinal-momentum distribution [a]

Range of x^2	α	α' (GeV^{-2})
0.00–0.01	$18.0^{+6.0}_{-4.0}$	$8.3^{+2.8}_{-1.9}$
0.00–0.09	11.9 ± 1.0	5.5 ± 0.45
0.09–0.40	7.0 ± 1.2	3.25 ± 0.55
0.35–0.64	5.3 ± 1.0	2.45 ± 0.45

2. Fits to the transverse-momentum distribution [b]

Range of p_T^2 (GeV^2)	β (GeV^{-2})
0.0–0.1625	7.0 ± 0.5
0.1625–0.3625	5.5 ± 0.6
0.3625–1.0	4.2 ± 0.4

3. Fits to the double-differential distributions [c]

Range of p_T (GeV)	Range of x^2	α	α' (GeV^{-2})
0.0–0.2	0.00–0.09	14.0 ± 1.5	6.5 ± 0.7
	0.09–0.30	9.4 ± 1.2	4.35 ± 0.55
	0.30–0.64	4.3 ± 1.3	2.0 ± 0.6
0.2–0.4	0.00–0.09	14.0 ± 1.0	6.5 ± 0.45
	0.09–0.30	7.4 ± 0.8	3.4 ± 0.4
	0.30–0.64	$6.5^{+1.6}_{-1.1}$	$3.0^{+0.75}_{-1.9}$
0.4–0.6	0.00–0.1225	11.0 ± 1.1	5.1 ± 0.5
	0.1225–0.64	6.5 ± 1.2	3.0 ± 0.55
0.6–0.8	0.00–0.0225	15.4 ± 6.6	7.1 ± 3.1
	0.0225–0.64	7.0 ± 0.5	3.25 ± 0.25
0.8–1.0	0.00–0.09	10.0 ± 3.1	4.65 ± 1.4
	0.09–0.64	5.3 ± 0.9	2.45 ± 0.4

[a] See Eq. (2a) for explanation of fit.
[b] See Eq. (2b) for explanation of fit.
[c] See Eq. (2c) for explanation of fit.

more sharply with increasing $|x|$.

In addition, in the absence of theory, we have attempted to parametrize our single-particle distributions, purely empirically. This parametrization, we feel should be useful in describing the data in a compact way. We have found that we can fit the momentum distributions with a series of Gaussians in x and p_T, of the form:

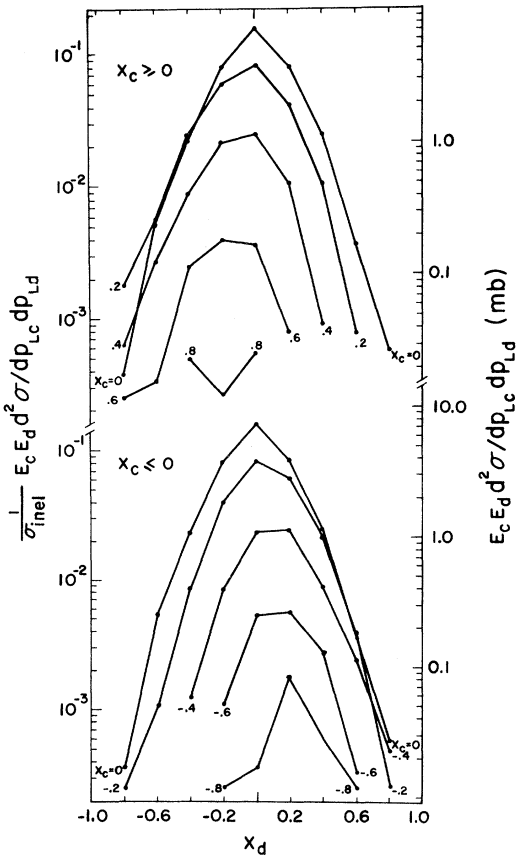

FIG. 9. The two-particle longitudinal-momentum distributions g and g_N defined in the text, as a function of x_d, for selected intervals of x_c of width $\Delta x_c = 0.2$. The plots are symmetrized so that there are two entries per pion pair.

$$E\frac{d\sigma}{dp_L} \propto \exp(-\alpha x^2) = \exp(-\alpha' p_L^2), \tag{2a}$$

$$\pi^{-1}E\frac{d\sigma}{dp_T^2} \propto \exp(-\beta p_T^2), \tag{2b}$$

$$\pi^{-1}E\frac{d^2\sigma}{dp_T^2 dp_L} \propto \exp[-\alpha(p_T)x^2] = \exp[-\alpha'(p_T)p_L^2]. \tag{2c}$$

The data and fitted curves are shown in Figs. 6, 7, and 8; the parameters of the fits, performed by

TABLE III. Some relevant quantities in $\bar{p}n \to 2\pi^+ X$.

Pair-production cross section	$\sigma(2\pi^+)$	13.5 ± 0.75 mb [a]
2nd moment of multiplicity distribution	$\langle n^2 - n\rangle = 2\sigma(2\pi^+)/\sigma_{tot}$	0.40 ± 0.04
Same, relative to σ_{inel}	$\langle n^2 - n\rangle_{inel} = 2\sigma(2\pi^+)/\sigma_{inel}$	0.57 ± 0.06
Correlation integral	$\Gamma = \langle n^2 - n\rangle - \langle n\rangle^2$	0.17 ± 0.06
Same, relative to σ_{inel}	$\Gamma_{inel} = \langle n^2 - n\rangle_{inel} - \langle n\rangle_{inel}^2$	0.11 ± 0.11

[a] Including 9 and more prongs.

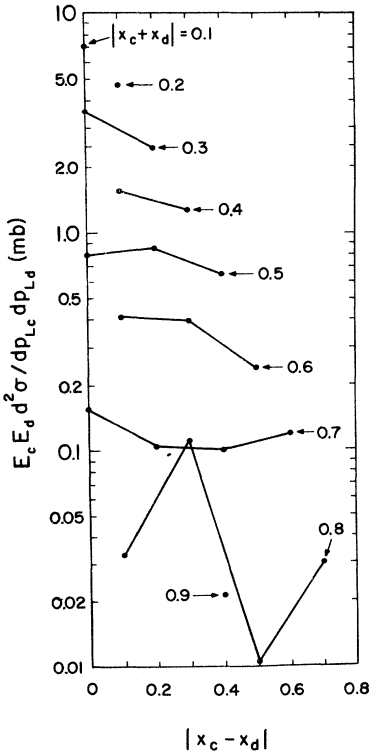

FIG. 10. The two-particle longitudinal-momentum distribution g, as a function of $|x_c - x_d|$, for selected intervals of $|x_c + x_d|$ of width $\Delta|x_c + x_d| = 0.1$. Only these pion pairs where both are in the same hemisphere are included.

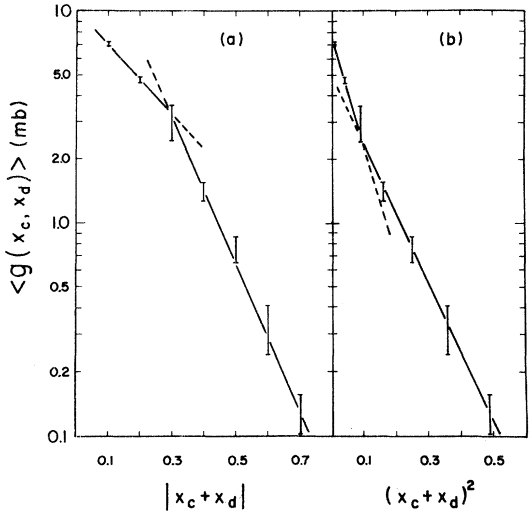

FIG. 11. The two-particle longitudinal-momentum distribution g, averaged over $|x_c - x_d|$, as a function of (a) $|x_c + x_d|$ and (b) $(x_c + x_d)^2$. Only those pion pairs where both are in the same hemisphere are included. The solid lines are the results of the fits described in the text.

TABLE IV. Fits to g vs $|x_c+x_d|$.

Fit		Value of parameter
$g \propto \exp(-\gamma\|x_c+x_d\|)$	$0.0 < \|x_c+x_d\| < 0.3$	$\gamma = 3.8^{+0.6}_{-0.4}$ GeV^{-1}
	$0.3 < \|x_c+x_d\| < 0.7$	$\gamma = 8.0 \pm 0.9$ GeV^{-1}
$g \propto \exp[-\gamma'(x_c+x_d)^2]$	$0.0 < \|x_c+x_d\| < 0.3$	$\gamma' = 12.3^{+2.2}_{-0.6}$ GeV^{-2}
	$0.3 < \|x_c+x_d\| < 0.7$	$\gamma' = 7.55 \pm 0.75$ GeV^{-2}

graphical methods, are displayed in Table II. Note the clean breaks in the slopes; $x \simeq 0.3$ ($x^2 \simeq 0.09$) appears to be a transition point, at least when $p_T \lesssim 0.4$ (75% of the events).

V. TWO-PARTICLE DISTRIBUTIONS AND CORRELATIONS

First we list in Table III the definitions and values of certain over-all quantities (integrated over phase space) which are used to describe two-particle production. The surprising feature is the positive correlation found, $\Gamma > 0$, while in other reactions,[15,16,17] the correlation is $\Gamma \lesssim 0$ below 30-GeV/c incident momentum, presumably due to energy-momentum conservation.[18]

Now we turn to the two-particle longitudinal-momentum distribution

$$g(x_c, x_d) = E_c E_d \frac{d^2\sigma}{dp_{Lc}\,dp_{Ld}},$$

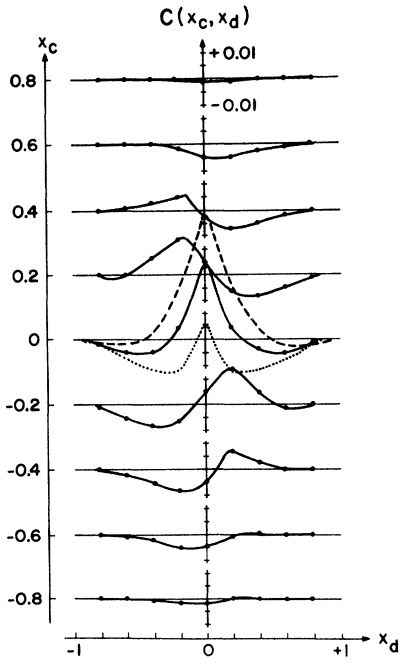

FIG. 12. The two-particle longitudinal correlation function C defined in the text, as a function of x_d, for selected intervals of x_c of width $\Delta x_c = 0.2$. Solid line, C is normalized by $\sigma_{inel} = 47$ mb; dashed line, C normalized by $\sigma_{tot} = 68$ mb; dotted line, C normalized by $\sigma_{tot}(\infty) = 40$ mb.

which, like the single-particle distribution can be normalized to either the total or the inelastic cross section. Again we use

$$g_N(x_c, x_d) = g(x_c, x_d)/\sigma_{\text{inel}} .$$

We plot in Fig. 9 the distributions g and g_N as a function of x_c and x_d. An interestingly simpler pattern appears in Fig. 10 where g is plotted as a function of $|x_c + x_d|$ and $|x_c - x_d|$, for those pairs where x_c and x_d have the same sign. In this case, as noted[19] in other reactions at moderately high energies, g is nearly independent of $|x_c - x_d|$, and depends mostly on $|x_c + x_d|$. A striking peak does appear at $x_c - x_d = 0$, when g is integrated over $|x_c + x_d|$ (not shown), as in $K^+p \to 2\pi^-$ at higher energy,[20] but it is clear that in our case it could be a kinematic reflection of a peak at $|x_c + x_d| \simeq 0$. However these considerations are too qualitative to draw any conclusion about the presence or absence of correlation, a question treated further in the next paragraph. To describe quantitatively the $|x_c + x_d|$ dependence of g, we have plotted that function averaged over $|x_c - x_d|$, as a function of $|x_c + x_d|$ in Fig. 11, and attempted different fits to the data. As in the case of the single-particle distributions, power-law parametrizations fail, but a superposition of two exponentials, or two Gaussians, gives a reasonable fit. The results are given in Table IV; notice, as in the single-particle distributions, the break is at $x \simeq 0.3$.

To terminate the subject of two-particle effects, we plot in Fig. 12 the correlation function

$$C(x_c, x_d) = g_N(x_c, x_d) - f_N(x_c) f_N(x_d)$$
$$= \sigma^{-1}[g(x_c, x_d) - \sigma^{-1} f(x_c) f(x_d)],$$

where σ is σ_{tot} or σ_{inel} . It is clear that the magnitude and the sign of the correlation depend critically on the normalization cross section. Some authors,[21] in view of the existence of strong kinematic correlations[22] choose a definition such that their integrated correlation

$$\iint C'(x_c, x_d) dx_c \, dx_d = 0.$$

Similarly, we prefer the σ_{inel} normalization because it gives an integrated correlation which is compatible with zero within errors (see Table III), and appears to us more "reasonable." However, we have indicated in one of the curves of Fig. 12 the effect of alternate normalizations. In addition to the expected negative correlations due to energy-momentum conservation, there appears a very strong positive peak[23] at $x_c \simeq x_d \simeq 0$. A qualitatively similar effect has been observed in a number of inclusive reactions: $\pi^+p \to 2\pi^-$ at 18 GeV/c,[24] in $K^+p \to 2\pi^-$ at 11.8 GeV/c,[20] and $\pi^-p \to$ any pair at 60 GeV/c and $pp \to$ any pair at 67 GeV/c.[16]

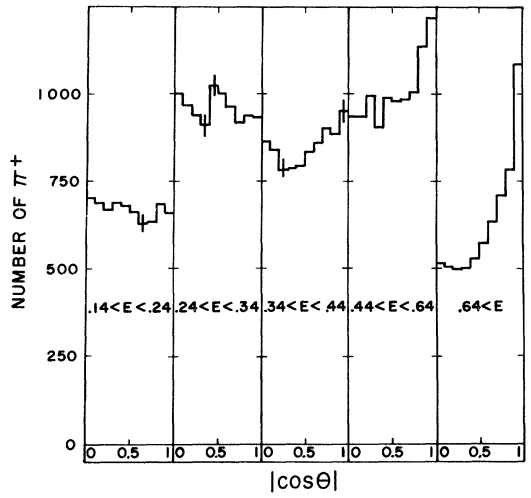

FIG. 13. Angular distribution of positive pions for five different slices of energy. The distributions are folded about $\cos\theta = 0$.

VI. THERMODYNAMIC BEHAVIOR

In the case where the angular distribution of produced particles were isotropic in the center of mass (this situation would correspond, in Hagedorn's model,[4] to the case where all "fireballs" are at rest in the c.m. system), one could expect the energy E of these particles to be distributed (for bosons), according to the Bose-Einstein formula $[\exp(E-\mu)/T - 1]^{-1}$, where μ is the chemical potential and T the temperature provided that,

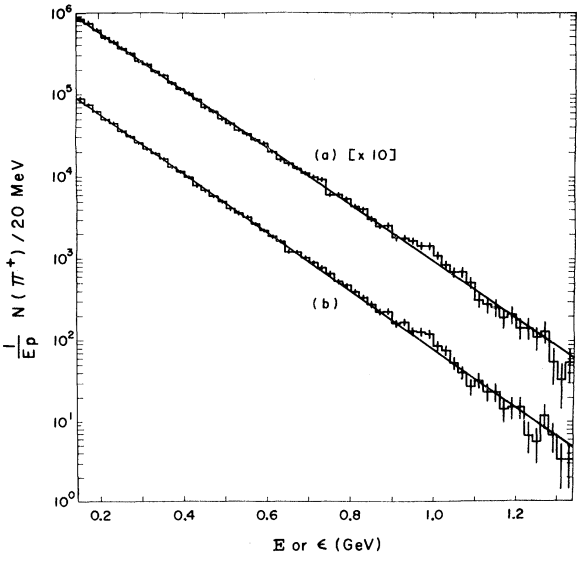

FIG. 14. Number of positive pions, weighted by the factor $1/pE$, plotted as a function of (a) the energy E, and (b) the quantity $\epsilon = [\lambda^2 p_L^2 + p_T^2 + m_\pi^2]^{1/2}$ with $\lambda = 0.9306$. For (a) the data have been multiplied by 10 to separate the curves. The solid line is the Boltzmann fit in each case.

TABLE V. Results of thermodynamic fits.

Distribution	λ	Temperature (MeV)	Chemical potential (MeV)	χ^2/d
Boltzmann	1.0	125.80 ± 0.27	···	1.28
Bose-Einstein	1.0	131.32 ± 0.30	0 [a]	2.20
Bose-Einstein	1.0	126.99 ± 0.28	-176 ± 17	1.24
Boltzmann	0.9306	122.01 ± 0.26	···	1.09
Bose-Einstein	0.9306	127.15 ± 0.29	0 [a]	1.87
Bose-Einstein	0.9306	123.23 ± 0.27	-160 ± 16	1.04

[a] Constrained value.

as stated in the Introduction, the energy available for particle creation is large compared to the temperature. Note that this "energy available for particle creation" is not generally the same as the total c.m. energy because of the well-known tendency of at least some of the particles to carry large longitudinal momenta.

A check with Fig. 13 shows that there is some anisotropy for fast pions in our data. To take into account this generally observed fact in terms of a single parameter, λ, Hoang[25] has proposed the replacement

$$p_L \to p'_L = \lambda p_L ,$$

$$p \to p' = (p'^2_L + p_T^2)^{1/2},$$

$$\cos\theta \to \cos\theta' = p'_L/p' ,$$

$$E \to \epsilon = (p'^2_L + p_T^2 + m_\pi^2)^{1/2}.$$

Then if λ is adjusted so that $\cos\theta'$ is isotropic, the distribution of ϵ should be given by the Bose-Einstein formula. This transformation of variables is possible if the data can be fit to the form

$$\Phi(\theta, \lambda) = \lambda[\,1 + (\lambda^2 - 1)\cos^2\theta\,]^{-3/2} .$$

If we combine the angular distributions of Fig. 13 and fit to this formula, we get a best fit with $\lambda = 0.9306 \pm 0.0037$, but with $\chi^2 = 32$ for nine degrees of freedom. There is more structure than Hoang's prescription can accomodate, but at least some of the departure from isotropy is represented.

We plot in Fig. 14 the appropriately weighted differential cross section as a function of E ($\lambda = 1$, data multiplied by 10) and of ϵ ($\lambda = 0.9306$). We fitted these data to the Bose-Einstein distribution, with the chemical potential being either fixed ($\mu \to -\infty$, i.e., the Maxwell-Boltzmann limit, or $\mu = 0$ as in the case of a photon gas), or with μ left as an additional free parameter besides temperature. The results are listed in Table V, where we see that we get good fits in all cases except when μ is constrained to be zero. Optimizing the value of λ helped the fit moderately; using Bose-Einstein with the chemical potential as an extra free parameter helped the fit very little.

The most remarkable feature however is the good agreement between those simple thermodynamic functions and the data over five orders of magnitude. This excellent fit suggests that the main features of the momentum distributions presented above in Sec. IV are merely reflections of thermodynamics, apart from a certain amount of "stretching" of the longitudinal momentum accounting for the angular anisotropy.

VII. ACKNOWLEDGMENTS

We are very grateful to Dr. L. Voyvodic, the ZGS, and 30-in. Bubble Chamber crews at Argonne for making this experiment possible, as well as to the scanning, measuring, and computing staffs at Ohio University. In addition, we are indebted to Dr. A. N. Diddens for sending unpublished data and Dr. R. C. Arnold for a very useful conversation.

*Research supported partly by the National Science Foundation.

†Present address: Centre de Recherches de l'Energie (I.N.R.S.), C. P. 1020, Varennes, Quebec, Canada.

‡Present address: Notre Dame University, South Bend, Indiana.

§Present address: Case-Western Reserve University, Cleveland, Ohio.

‖Present address: Martin-Marietta Company, Orlando, Florida.

[1]For recent reviews see W. R. Frazer, L. Ingber, C. H. Mehta, C. H. Poon, D. Silverman, K. Stowe, P. D. Ting, and H. J. Yesian, Rev. Mod. Phys. 44, 284 (1972), and D. Horn, Phys. Rep. 4C, 1 (1972).

[2]Chan Hong-Mo, C. S. Hsue, C. Quigg, and Jiunn-Ming Wang, Phys. Rev. Lett. 26, 672 (1971).

[3]There is a $\bar{p}d$ bubble-chamber exposure at 15 GeV/c by the Rutgers-Strasbourg groups, Bull. Am. Phys. Soc. 17, 586 (1972).

[4]R. Hagedorn, Nucl. Phys. B24, 93 (1970), and references therein.

[5]B. G. Reynolds, K. E. Weaver, J. M. Bishop, D. O. Huwe, and J. A. Malko, Phys. Rev. D 2, 1767 (1970).

[6]M. A. Ijaz, B. A. Munir, and E. J. B. Terreault, Nucl. Phys. B42, 85 (1972).

[7]As interpolated by the authors of Ref. 5. The error stated there did not include the normalization error, but we do include it here.

[8]B. Musgrave, in *Phenomenology in Particle Physics*, edited by C. Chiu, G. Fox, and A. J. G. Hey (California Institute of Technology, Pasadena, 1971), p. 467.

[9]R. C. Arnold, Argonne National Laboratory Report No.

ANL/HEP 7139, 1971 (unpublished).
[10]W. D. Shepard, J. T. Powers, N. N. Biswas, N. M. Cason, V. P. Kenney, R. R. Riley, D. W. Thomas, J. W. Elbert, and A. R. Erwin, Phys. Rev. Lett. 27, 1164 (1972). There are also data with somewhat lower statistics from D. J. Crennell *et al.*, Phys. Rev. Lett. 28, 643 (1972).
[11]S. Stone, T. Ferbel, P. Slattery, and B. Werner, Phys. Rev. D 5, 1621 (1972).
[12]Winston Ko and Richard L. Lander, Phys. Rev. Lett. 26, 1064 (1971).
[13]J. V. Allaby *et al.*, CERN report (unpublished); and A. N. Diddens, private communication.
[14]E. Flaminio, J. D. Hansen, D. R. O. Morrison, and N. Tovey, CERN Report No. CERN/HERA 70-3, 1970 (unpublished).
[15]E. L. Berger, B. Y. Oh, and G. A. Smith, Phys. Rev. Lett. 29, 675 (1972).
[16]K. Fialkowski, K. Rybicki, and R. Witt, Nucl. Phys. B44, 509 (1972).
[17]G. R. Charlton *et al.*, Phys. Rev. Lett. 29, 515 (1972).
[18]$\Gamma \simeq 0$, however, if one uses the asymptotic cross section $\sigma_{tot}(\infty) = 40$ mb, instead of the cross section at 3.5 GeV/c as a normalization.
[19]C. Quigg, Jiunn-Ming Wang, and Chen Ning Yang, Phys. Rev. Lett. 28, 1290 (1972).
[20]Winston Ko, Phys. Rev. Lett. 28, 935 (1972).
[21]J. V. Beaupre *et al.*, Phys. Lett. 40B, 510 (1972).
[22]M. Kugler and R. G. Roberts, Weizmann Inst. Report No. WIS 71/51, 1971 (unpublished).
[23]Note however that the peak vanishes with the normalization $\sigma_{tot}(\infty)$; see also Ref. 18.
[24]W. D. Shepard, J. T. Powers, N. N. Biswas, N. M. Cason, V. P. Kenney, and D. W. Thomas, Phys. Rev. Lett. 28, 703 (1972).
[25]T. F. Hoang, D. Rhines, and W. A. Cooper, Phys. Rev. Lett. 27, 1681 (1971).

PHYSICAL REVIEW D VOLUME 8, NUMBER 7 1 OCTOBER 1973

$\bar{p}p$ Elastic Scattering at 2.85 GeV/c

H. B. Crawley, E. S. Hafen, and W. J. Kernan
Ames Laboratory-USAEC and Department of Physics, Iowa State University, Ames, Iowa 50010
(Received 7 May 1973)

$\bar{p}p$ elastic scattering at an incident beam momentum of 2.85 GeV/c is analyzed using 18 412 events. The simple exponential parametrization of the diffraction peak is found to be a poor representation of the data. Two other parametrizations are tried and the estimates of $d\sigma/dt$ at $t = 0$ and of the slope of the diffraction peak are found to differ significantly between various parametrizations. It is found that two coherent interfering exponentials are able to represent the differential cross section over the range $0.04 \leq |t| \leq 1.8$ (GeV/c)^2 with a χ^2 probability of approximately 40%.

In elastic scattering the parametrization can be important in obtaining an estimate of the differential cross section at $t = 0$. Above 1.5 GeV/c incident beam momentum, the parametrization which has normally been used in $\bar{p}p$ elastic scattering represents a limited region of the diffraction peak with a simple exponential:

$$\frac{d\sigma}{dt} = \left(\frac{d\sigma}{dt}\right)_0 e^{bt} . \quad (1)$$

In one of the experiments, Parker *et al.*[1] concluded after studying this reaction from 1.5 to 2.9 GeV/c that " ...no significant consistent improvement in the fits is realized by allowing curvature in the very low-t region." In a more recent experiment, Ambats *et al.*[2] include a curvature term; that is, they use $\exp(bt + ct^2)$ in analyzing their data from 3 to 6 GeV/c.

We have measured the differential cross section for $\bar{p}p$ elastic scattering at 2.85 GeV/c using the 31-in. bubble chamber and a separated beam at the Brookhaven AGS. The present analysis is based on 18 412 events which are in a limited fiducial volume and which satisfy the elastic scattering hypothesis with a χ^2 less than 12. The resulting differential cross sections are presented in Table I for the t range $0.04 \leq |t| \leq |t_{max}|$ in (GeV/c)^2, where $t_{max} \approx -4.0$ (GeV/c)^2. The data for the diffraction peak region, that is, $0.04 \leq |t| \leq 0.45$ (GeV/c)^2, have been plotted in Fig. 1. For $|t| < 0.240$ (GeV/c)^2 the bin size used is 0.0050 (GeV/c)^2, which is significantly larger than the resolution. At larger t the bin size has been increased to keep the statistical errors small.

An attempt to fit the limited t range $0.04 \leq |t| \leq 0.25$ (GeV/c)^2 to Eq. (1) was made. The resulting fit is relatively poor with a χ^2/ν of 1.39 or a χ^2 probability of approximately 5%. It should be noted, however, that the resulting parameters agree quite well with those given for this parametrization for data from other experiments at nearby energies. Another indication of the poor fit is the variation in the slope parameter, and the intercept as the t range of the data used in the determination